International Journal of Adhesion & Adhesives 113 (2022) 103071

Contents lists available at ScienceDirect

International Journal of Adhesion and Adhesives

journal homepage: www.elsevier.com/locate/ijadhadh

Tangential bond stiffness evaluation of adhesive lap joints by spectral interference of the low-frequency A0 lamb wave

Naoki Mori [a,*], Daichi Wakabayashi [b], Takahiro Hayashi [a]

[a] Department of Mechanical Engineering, Graduate School of Engineering, Osaka University, Japan
[b] Division of Mechanical, Materials and Manufacturing Science, School of Engineering, Osaka University, 2-1 Yamadaoka, Suita, Osaka, 565-0871, Japan

ARTICLE INFO

Keywords:
Non-destructive testing
Interfaces
Guided wave
Ultrasonic spectroscopy

ABSTRACT

Transmission spectra of the lowest-order antisymmetric (A0) Lamb wave for adhesively bonded single lap joints are experimentally investigated in a frequency range below 0.4 MHz. Based on the theoretical results of the wave interference, a tangential bond stiffness evaluation method is proposed for the lap joints. Aluminum alloy plates bonded with epoxy adhesive on different conditions were prepared as bonded specimens. An air-coupled ultrasonic transducer was used to generate the A0 mode in the specimens, and the signals of the transmitted waves across the joints were measured with a pin-type piezoelectric transducer. Spectral analysis was performed for the measured waveforms, and the transmission coefficient was calculated for each specimen as a function of frequency. The experimental results showed that the transmission coefficient has local maxima and minima at multiple frequencies, called peak and notch frequencies, respectively. The sets of the peak and notch frequencies were different among the bonded specimens. Based on the peak and notch frequencies, the tangential bond stiffness was estimated for each bonded specimen. As a result, the bond stiffnesses obtained for the specimens with the same nominal bond thickness and adherend pretreatment were almost equal even if the bond lengths were different. Furthermore, the evaluation results showed that pretreatments such as sanding and contamination of adherend surfaces affect the bond stiffness due to the change in the interfacial stiffness.

1. Introduction

Adhesive bonding contributes to weight reduction in the joining of components in various structures such as automobiles and aircraft. Non-destructive testing (NDT) for adhesively bonded joints often aims to detect defects in the joints, e.g. voids and cracks [1,2]. Ultrasonic waves, which are one of the NDT tools for adhesive joints, have the potential not only for the defect detection but also for the evaluation of cohesive and adhesive properties. Different ultrasonic techniques were proposed in previous studies to estimate the bulk property of adhesive and the interfacial property between adhesive and adherend [3–6].

Guided waves enable wide-range inspection owing to the capability of relatively long propagation distances compared to bulk waves. One of the guided waves propagating in thin plates, called Lamb waves, is often utilized for inspection of thin-walled structures. Numerous studies were carried out so far for the characterization of adhesive joints with guided waves including Lamb waves. An effective approach is the measurement of the dispersion relations of guided waves propagating in adhesive joints [7–9]. The dispersion relations are obtained by measuring wavefields at multiple locations on the joint, which usually makes the experimental procedure time-consuming and complicated. Another approach is the measurement of transmitted guided waves across overlap joints [10–16]. The properties of the joint are estimated based on the transmission characteristics of the guided modes. Lamb waves in isotropic elastic plates are classified into two types of modes, symmetric (S) and antisymmetric (A) modes, from the viewpoint of the deformation profiles along the thickness direction. Many researchers including Rokhlin [10], Lowe et al. [11], and Lanza di Scalea et al. [12] examined the transmission of the lowest-order symmetric (S0) and antisymmetric (A0) Lamb modes across single lap joints.

In recent years, Mori and Kusaka [14] have theoretically investigated the peak behavior of the transmission coefficient at single lap joints for the A0 mode incidence. This phenomenon occurs due to the constructive interference of directly transmitted wave and multiply reflected waves from the overlap region. When an adhesive joint is modeled by a spring-type interface [17–19], it has been shown that the peak frequencies in a low frequency range depend on the tangential stiffness of the joint, nominally not on the normal stiffness [14]. The transmission

* Corresponding author.
E-mail address: n.mori@mech.eng.osaka-u.ac.jp (N. Mori).

https://doi.org/10.1016/j.ijadhadh.2021.103071
Received 7 August 2021; Received in revised form 14 November 2021; Accepted 20 November 2021
Available online 10 December 2021

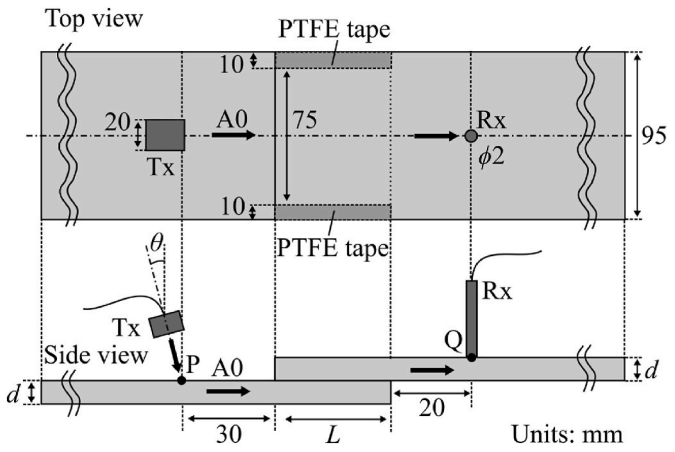

Fig. 1. Schematic of bonded specimen and experimental setup.

Table 1
Adherend surface pretreatment for bonded specimens.

Specimens	Surface pretreatment
S30 & S20	Sanding with abrasive papers
C30	Contaminated by silicone oil
R30	N/A

coefficient similarly takes local minima at multiple frequencies, which are called notch frequencies. The above results suggest that the tangential stiffness of single lap joints can be estimated by measuring the peak and notch frequencies in the Lamb wave transmission spectrum. The theoretical results have also shown that the viscoelastic attenuation by adhesive does not significantly affect the peak frequencies [14]. This feature is favorable because *a priori* knowledge about the wave attenuation property of adhesive is not necessary for the stiffness evaluation. However, the spectrum characteristics of the Lamb wave transmission across single lap joints have not been fully investigated in experiments. Further understanding of the spectrum characteristics will enable the estimation of bond stiffness for lap joints with Lamb waves, which remains a challenge at present.

The aim of this study is to examine the local maxima and minima behavior of the Lamb wave transmission spectra for adhesively bonded single lap joints. Based on the theoretical results of the peak and notch frequencies, a tangential bond stiffness evaluation method is proposed and applied to different bonded specimens.

This paper is structured as follows. In Section 2, bonded specimens used in the study are described, and procedures for the Lamb wave measurement are explained. In Section 3, theoretical backgrounds are summarized based on the previous paper [14], and a bond stiffness evaluation method is proposed. In Section 4, measured waveforms are shown and the transmission coefficients are calculated by spectral analysis. In Section 5, the bond stiffness is estimated for each bonded specimen with the proposed method. The effects of the bond length and the surface pretreatment on the estimation results are discussed.

2. Experiment

2.1. Bonded specimens

The schematic of a bonded lap joint used in this study is shown in Fig. 1. Two rectangular-shaped A5052 aluminum alloy plates of width 95 mm, length 200 mm, and thickness $d = 2.0$ [mm] were bonded by a two-component epoxy adhesive (TB2082C, ThreeBond Co., Ltd.) to fabricate a single lap joint.

Four bonded specimens, namely, reference (R30), contaminated (C30), and two sanded (S30 and S20) specimens, were produced in this study. In order to control bond thickness, polytetrafluoroethylene (PTFE) tapes of width 10 mm were put on a part of a bonding surface, as shown in Fig. 1. The pretreatment of adherends for the four specimens is summarized in Table 1. Specimens S30 and S20 correspond to the specimens whose adherend surfaces were sanded by abrasive papers of #80 before bonding. A preliminary measurement showed that the sanded surfaces had the arithmetic average roughness Ra = 1.1 μm and the average maximum height Rz = 4.6 μm. For specimen C30, silicone spray (No. 1420, Kure Engineering Ltd.) was applied on a bonding surface. The nominal amount of the applied silicone oil was 0.2 g/cm^2. Specimen R30 is a reference specimen, which was produced with no additional surface pretreatment.

Table 2
Dimensions of the bonded specimens (units: mm).

Specimens	Bond length L	Bond thickness h
S30	30.0	0.10
R30	30.0	0.11
C30	30.0	0.10
S20	20.0	0.10

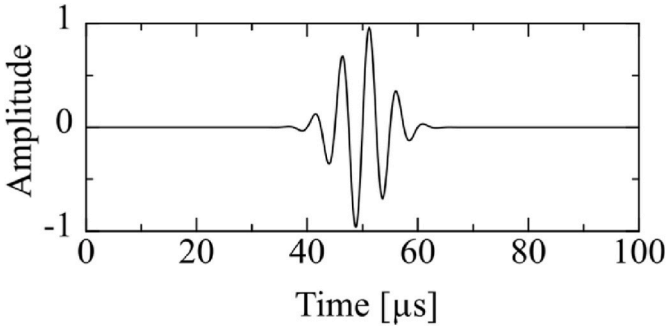

Fig. 2. Input waveform for the arbitrary waveform generator.

The dimensions of the produced specimens are given in Table 2. The bond lengths L of specimens S30, R30, and C30 were $L = 30.0$ [mm], while that of specimen S20 was $L = 20.0$ [mm]. To measure the bond thickness h of each specimen, the side faces of the overlapped part were polished and observed by an optical microscope. As shown in Table 2, the bond thicknesses h of specimens S30, C30, and S20 were $h = 0.10$ [mm], while that of specimen R30 was slightly thicker, $h = 0.11$ [mm].

2.2. Lamb wave measurement

Ultrasonic measurement was carried out for the normal incidence of the A0 Lamb wave on single lap joints. The experimental setup is schematically shown in Fig. 1. A gaussian modulated sinusoidal wave

$$g(t) = \exp\left[-\left(\frac{t-t_0}{s_0}\right)^2\right]\sin[2\pi f_0(t-t_0)] \tag{1}$$

was input into a Keysight arbitrary waveform generator 33511B, where t is time, $f_0 = 0.2$ [MHz] is the center frequency, $t_0 = 50$ [μs], and $s_0 = 6$ [μs]. The input waveform is shown in Fig. 2. The output voltage from the arbitrary waveform generator was amplified by an NF bipolar amplifier BA4825 and sent into an air-coupled ultrasonic transducer (0.4K14 × 20 N, Japan Probe Co., Ltd.). The transducer has a rectangular cross-section with a width of 20 mm and a length of 14 mm. The ultrasonic wave pulse emitted from the air-coupled transducer was incident obliquely on a specimen at location P, as indicated in Fig. 1. To generate the A0 mode in the plate, the incident angle θ was determined by Snell's law

$$\frac{\sin\theta}{c_0} = \frac{1}{c_{A0}}, \tag{2}$$

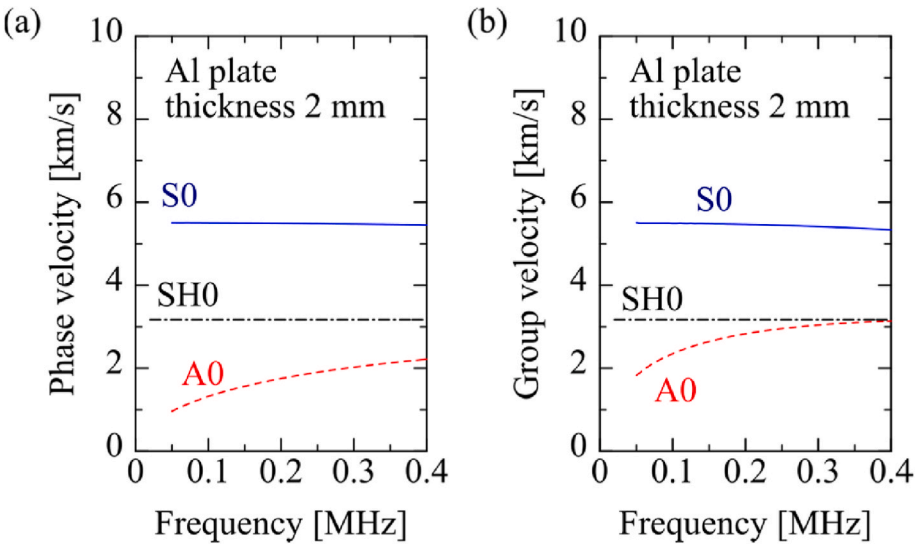

Fig. 3. Dispersion curves of guided wave modes: (a) phase velocity and (b) group velocity.

where $c_0 = 0.34$ [km/s] is the sound velocity of air, and c_{A0} is the phase velocity of the A0 mode, which depends on frequency. The phase velocity and the group velocity of different guided wave modes in 2 mm thick aluminum alloy plates, i.e. Lamb modes and shear horizontal (SH) guided modes, were theoretically obtained by solving the dispersion relations [20]. The obtained dispersion curves are shown in Fig. 3(a) and (b). The phase velocity of the A0 mode at 0.2 MHz is $c_{A0} = 1.8$ [km/s]. By substituting this into Eq. (2), the incident angle for the A0 mode generation is calculated to be $\theta = 11$ [deg]. The distance of the path between the air-coupled transducer and the specimen was 12.0 mm.

A pin-type piezoelectric transducer (VP-1093, Valpey Fisher, diameter 2.3 mm, nominal frequency 1.2 MHz) was used to detect the out-of-plane vibration in a relatively wide frequency range at location Q, indicated in Fig. 1. The pin-type transducer was coupled to the specimen by an acoustic couplant (B2, Olympus). The received signal was passed in a 0.02–1 MHz band pass filter and amplified by a RITEC broadband receiver BR-640A. The output signal was recorded as digital data by an oscilloscope (HDO4034A, Teledyne LeCroy), which were transferred to a PC after averaging over 100 synchronized signals. The arbitrary waveform generator and the oscilloscope were controlled by the PC via LabVIEW.

In the frequency range below 0.4 MHz, three guided wave modes, namely, the S0 and A0 Lamb modes, and the lowest-order shear horizontal (SH0) mode, can propagate in 2 mm thick aluminum alloy plates. Since the receiving transducer used in this study detects the out-of-plane vibration, the signals of the SH waves are not measured. Furthermore, the out-of-plane deformation of the A0 mode is dominant over the S0 mode at low frequency thickness products [20]. When the A0 mode is incident on an overlap region, the S0 mode is generated due to mode conversion. However, a preliminary investigation by two-dimensional (2D) theoretical analysis showed that in the frequency thickness product of the present study, the effect of the transmitted S0 mode on the waveforms is not significant if the out-of-plane vibration is measured. It can be therefore assumed that waveforms measured by the receiver represent the time histories of the A0 mode. It is shown later that wave packets corresponding to the S0 mode did not appear in the measured signal of the incident wave.

To obtain the spectrum of the incident wave before reaching the overlap region, a reference waveform was measured in a single plate region for each bonded specimen. The interval between the excitation and reception points was set to be 50 mm. Based on the group velocity of the A0 mode, the incident and transmission waveforms were extracted from the measured signals by tapered rectangular windows (Tukey windows). The tapered parts of the windows are expressed as cosine functions of time length 1 μs. The obtained waveforms were analyzed by fast Fourier transform (FFT). The amplitude spectra of the incident and transmission waveforms are denoted as $A_1(f)$ and $A_2(f)$, respectively, where f is frequency. For each bonded specimen, the transmission coefficient

$$T = \frac{A_2(f)}{A_1(f)}, \tag{3}$$

is calculated as a function of frequency f.

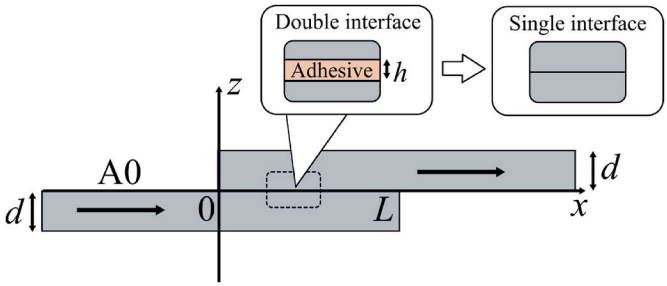

Fig. 4. Theoretical model of a single lap joint.

3. Tangential bond stiffness evaluation method for single lap joints

In this section, a tangential bond stiffness evaluation method for single lap joints is proposed based on the theoretical results in Ref. [14]. For this purpose, the theoretical backgrounds are explained here.

3.1. Theoretical model of lap joints

Fig. 4 shows the theoretical model of a single lap joint. In the Cartesian x-y-z coordinates, two homogeneous, isotropic, and linear elastic plates are bonded together. The two plates are semi-infinite and under a plane-strain condition in the x-z plane. The normal and shear stress components, $\sigma_z(x, z, t)$ and $\tau_{zx}(x, z, t)$, are determined by Hooke's law, and the displacement components $u_x(x, z, t)$ and $u_z(x, z, t)$ are governed by Navier's equation. The two plates have the same plate thickness d and material property. In this study, mass density $\rho = 2.7 \times 10^3$ [kg/m^3], longitudinal wave velocity $c_L = 6.40$ [km/s], and transverse wave

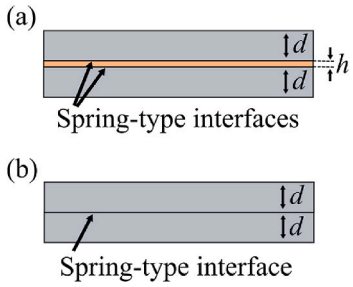

Fig. 5. (a) Tri-layer structure and (b) bi-layer structure for the model comparison.

velocity $c_T = 3.17$ [km/s] are used for the modeling of aluminum alloy adherends. The overlap region is $0 < x < L$, where L denotes the bond length.

The overlap region $0 < x < L$ corresponds to a tri-layer structure which consists of an adhesive layer sandwiched by two adherends. The adhesive layer is modeled as a homogeneous and isotropic layer of thickness h, mass density ρ_A, longitudinal wave velocity c_{LA}, and transverse wave velocity c_{TA}. An adhesive interface between adhesive and adherend is modeled by a spring-type interface [17–19]. The boundary condition at the interface is expressed by

$$\sigma_z(x, z_I, t) = K_{IN}\left[u_z\left(x, z_I^+, t\right) - u_z\left(x, z_I^-, t\right)\right], \tau_{zx}(x, 0^\pm, t) = K_T[u_x(x, 0^+, t) - u_x(x, 0^-, t)], \quad (4)$$

where $z = z_I$ is the location of the interface, and K_{IN} and K_{IT} are normal and tangential interfacial stiffnesses, respectively. The superscript $+$ $(-)$ represents the upper (lower) side of the interface. The boundary condition of Eq. (4) is applied to two interfaces, $z_I = 0$ and $z_I = h$. In the present study, this modeling is referred to as a double interface model.

If the frequency of the incident wave is low and the bond thickness h is sufficiently thin, the double interface model can be reduced to a single interface model [17–19]. Namely, the adhesive layer and the adhesive interfaces can be collectively modeled as a single spring-type interface [19]. In the case of guided wave propagation, the above approximation is expected to be valid if $|\alpha_A h| \ll 1$ and $|\beta_A h| \ll 1$, where $\alpha_A = \sqrt{(\omega/c_{LA})^2 - k^2}$ and $\beta_A = \sqrt{(\omega/c_{TA})^2 - k^2}$ are the thickness-direction wavenumbers of the partial wave components [20] in the adhesive layer, k is the wavenumber of the guided wave, and $\omega = 2\pi f$. Under this condition, the boundary conditions of Eq. (4) can be replaced to

$$\sigma_z(x, 0^\pm, t) = K_N[u_z(x, 0^+, t) - u_z(x, 0^-, t)], \tau_{zx}(x, 0^\pm, t) = K_T[u_x(x, 0^+, t) - u_x(x, 0^-, t)], \quad (5)$$

where K_N and K_T are normal and tangential bond stiffnesses given by

$$\frac{1}{K_N} = \frac{1}{K_{LN}} + \frac{2}{K_{IN}}, \quad \frac{1}{K_T} = \frac{1}{K_{LT}} + \frac{2}{K_{IT}}, \quad (6)$$

respectively, if the interfacial stiffnesses at the two interfaces are identical. The quantities K_{LN} and K_{LT} are expressed as $K_{LN} = \rho_A {c_{LA}}^2/h$ and $K_{LT} = \rho_A {c_{TA}}^2/h$, which correspond to normal and tangential stiffnesses of the adhesive layer, respectively. Since the wave propagation behavior in the overlap region is determined by the bond stiffnesses K_N and K_T, the layer stiffnesses and the interfacial stiffnesses cannot simultaneously be identified by the transmission characteristics. For example, the estimation of the interfacial stiffness K_{IT} requires not only the bond stiffness K_T but also the layer stiffness K_{LT} to be obtained.

3.2. Validation of single interface model

Prior to the proposal of a bond stiffness evaluation method, the single interface model is validated for the specimens used in this study. To this end, the dispersion relations of guided wave modes in tri-layer and bi-layer structures are compared.

Table 3
Interfacial stiffness values used in the double interface model.

	Interfacial stiffness [GPa/μm]
Case I	$K_{IN} = K_{IT} = 10$
Case II	$K_{IN} = 0.05$, $K_{IT} = 0.02$

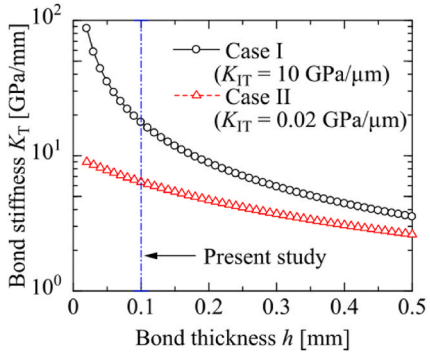

Fig. 6. Relation of the bond thickness and the tangential bond stiffness calculated by Eq. (6) in cases I and II. The bond thickness of the specimens used in this study is approximately 0.1 mm.

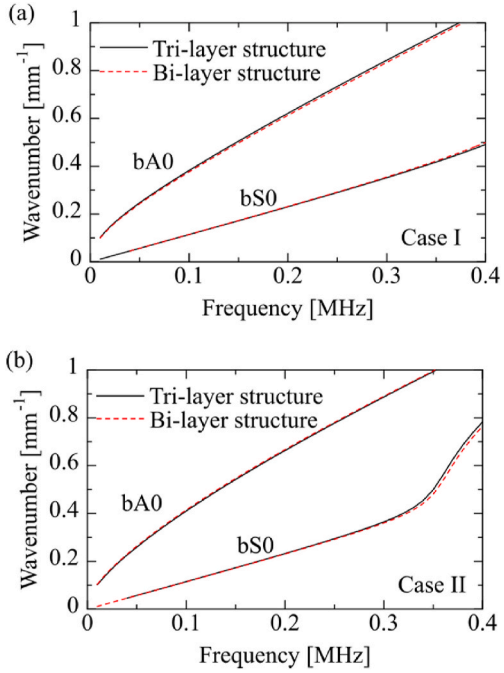

Fig. 7. Comparison of the dispersion curves of the guided waves for the tri-layer and bi-layer structures in (a) case I and (b) case II.

The schematics of the tri-layer and bi-layer structures are shown in Fig. 5(a) and (b), respectively. In the tri-layer structure, two adherends are coupled to an adhesive layer by two spring-type interfaces. This modeling is based on the double interface model, i.e. Eq. (4). The material property of the adhesive is assumed to be $\rho_A = 1.23 \times 10^3$ [kg/m^3], $c_{LA} = 2.7$ [km/s], and $c_{TA} = 1.2$ [km/s], which correspond to common epoxy-based adhesive. In accordance with the dimensions of the bonded specimens given in Table 2, the adherend thickness and the adhesive thickness are set as $d = 2$ [mm] and $h = 0.1$ [mm], respectively. On the other hand, the bi-layer structure corresponds to the single interface

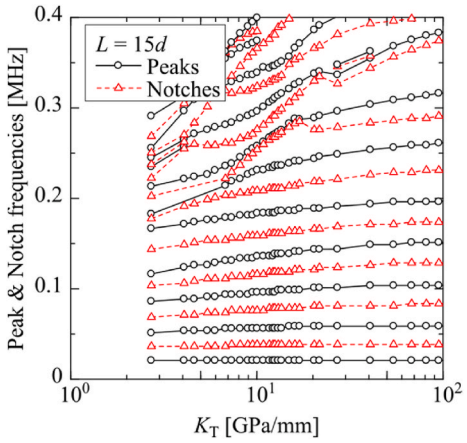

Fig. 8. Variation of the peak frequencies f_m^{pT} and notch frequencies f_m^{nT} of the A0 mode transmission coefficient with the tangential stiffness of an adhesive joint K_{T} at the bond length $L = 15d = 30$ [mm], obtained by theoretical analysis [14].

model, in which two adherends are directly joined by a spring-type interface. Under the plane-strain condition, the dispersion relations of Lamb type guided waves are theoretically calculated for both models [5, 14].

Two different cases are considered in the double interface model, as shown in Table 3. Case I represents the case of almost rigid adhesive interfaces, in which the interfacial stress and displacement components are continuous. On the other hand, the interfacial stiffnesses in case II correspond to weak adhesion, based on the interfacial stiffness estimated for specimen C30 in Section 5. By substituting K_{IN} and K_{IT} into Eq. (6), the normal and tangential bond stiffnesses K_{N} and K_{T} in the bi-layer structure are obtained. Fig. 6 shows the relations of the bond stiffness K_{T} to the bond thickness h in cases I and II. As the bond thickness increases, the contrast between the bond stiffnesses in the two cases is found to become ambiguous. For example, at $h = 0.4$ [mm], the bond stiffness is $K_{\mathrm{T}} = 4.3$ [GPa/mm] in case I and $K_{\mathrm{T}} = 3.0$ [GPa/mm] in case II. This fact suggests that the double interface model would be preferable for the modeling of thick adhesive layers. However, at the bond thickness of the specimens used in this study, i.e. $h = 0.1$ [mm], the two cases seem to be distinguishable. The bond stiffnesses in cases I and II are $K_{\mathrm{T}} = 17$ [GPa/mm] and $K_{\mathrm{T}} = 6.4$ [GPa/mm], respectively.

The wavenumbers of the guided waves in cases I and II are shown in Fig. 7(a) and (b), respectively. In both structures, the guided waves can be classified into symmetric (S) and antisymmetric (A) modes owing to the symmetry along the thickness direction. In a frequency range below 0.4 MHz, one symmetric (bS0) and one antisymmetric (bA0) mode propagate in each model. It is demonstrated in Fig. 7(a) and (b) that the dispersion curves for the tri-layer structure model are well reproduced by the bi-layer structure model. The maximum error between the dispersion curves of the two models was approximately 1%. This result shows that if the bond thickness is $h = 0.1$ mm and the incident frequency is lower than 0.4 MHz, the single interface model can be reasonably used for the modeling of the bonded specimens in the present study. At 0.4 MHz, the products of the wavenumber and the bond thickness for the A mode become $|\alpha_{\mathrm{A}}h| = 0.033$ and $|\beta_{\mathrm{A}}h| = 0.086$, which satisfy $|\alpha_{\mathrm{A}}h| \ll 1$ and $|\beta_{\mathrm{A}}h| \ll 1$.

3.3. Proposal of evaluation method based on theoretical results

In the theoretical analysis of Ref. [14], the monochromatic A0 plane wave was incident on a lap joint modeled by the single interface model. The theoretical results showed that in a low frequency range, the transmission coefficient of the A0 mode at the joint has local maxima and minima at multiple frequencies. The peak and notch frequencies

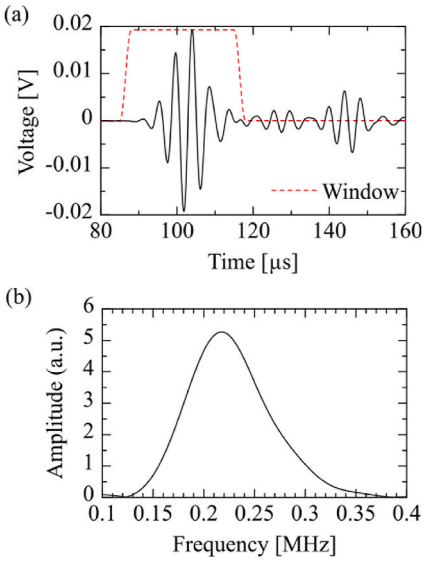

Fig. 9. (a) Reference waveform with a window function and (b) amplitude spectrum obtained by spectral analysis.

depend on the tangential stiffness K_{T}, nominally not on the normal stiffness K_{N} [14]. Fig. 8 shows the variation of the peak frequencies f_m^{pT} and the notch frequencies f_m^{nT} ($m = 1,2, \ldots$) with the tangential stiffness K_{T} at the bond length $L = 15d = 30$ [mm]. The peak and notch frequencies have different sensitivities to the tangential stiffness K_{T} probably because the variation of the dispersion relation of the bA0 mode with K_{T} depends on frequency. On the whole, the peak and notch frequencies tend to increase as the tangential stiffness K_{T} increases.

This feature implies that if the bond length L is known *a priori*, the tangential bond stiffness K_{T} can be estimated by measuring the peak and notch frequencies of the A0 mode transmission coefficient. The following function

$$J(K_{\mathrm{T}}) = \frac{1}{M_{\mathrm{p}}} \sum_{m=1}^{M_{\mathrm{p}}} \left[\frac{f_m^{\mathrm{pE}} - f_m^{\mathrm{pT}}(K_{\mathrm{T}})}{f_m^{\mathrm{pE}}} \right]^2 + \frac{1}{M_{\mathrm{n}}} \sum_{m=1}^{M_{\mathrm{n}}} \left[\frac{f_m^{\mathrm{nE}} - f_m^{\mathrm{nT}}(K_{\mathrm{T}})}{f_m^{\mathrm{nE}}} \right]^2 \tag{7}$$

is defined, where f_m^{pE} and f_m^{nE} are the experimental values of the peak and notch frequencies, respectively, and M_{p} and M_{n} are the numbers of the peak and notch frequencies, respectively. The tangential bond stiffness $K_{\mathrm{T}} = K_{\mathrm{T0}}$ which minimizes $J(K_{\mathrm{T}})$ is sought.

4. Experimental results

Reference waveforms were first measured in single plate regions of bonded specimens, as shown in Fig. 9(a). The measurement was repeated at least three times, and the relative variation of the peak voltages among the waveforms was approximately 4%. When the input waveform shown in Fig. 2 is used for the wave generation, the arrival times of the S0 and A0 modes at 0.2 MHz are predicted to be 94 μs and 103 μs, respectively, from the group velocities of the S0 (5.47 km/s) and A0 (2.83 km/s) modes. The estimate for the A0 mode is in good agreement with the arrival time of the first wave packet in the measured waveform, 102 μs. It is therefore suggested that the A0 mode was successfully generated by the air-coupled transducer. Subsequently, additional wave packets appeared at 127 μs and 145 μs in Fig. 9(a). These components correspond to reflected waves from edges.

To examine the frequency component of the direct A0 mode, the first wave packet was extracted by multiplying a tapered rectangular window shown in Fig. 9(a) and was analyzed by FFT. The amplitude spectrum is shown in Fig. 9(b). The amplitude spectrum had a maximum at around 0.22 MHz, showing smooth distribution in 0.15–0.35 MHz.

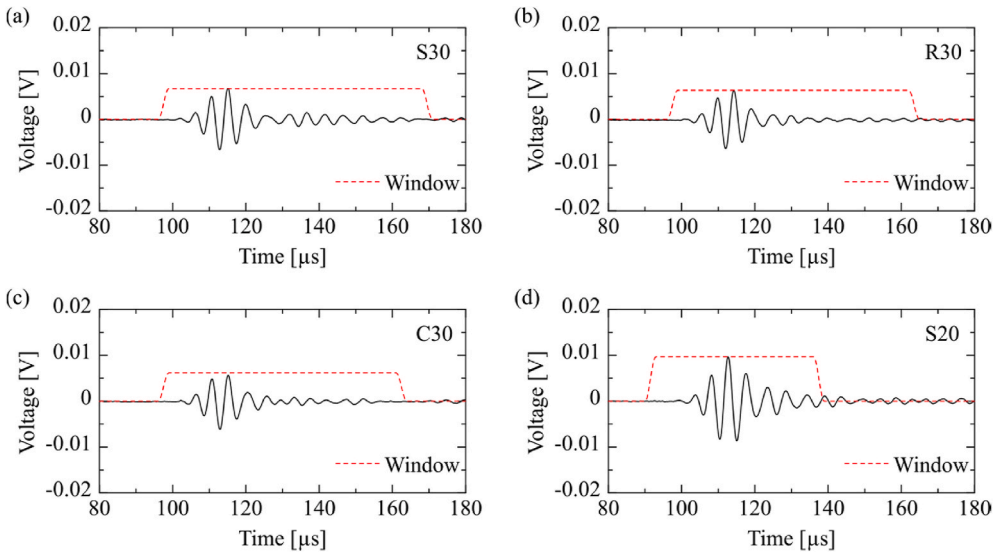

Fig. 10. Measured waveforms for specimens (a) S30, (b) R30, (c) C30, and (d) S20. Dashed lines represent window functions used in the spectral analysis.

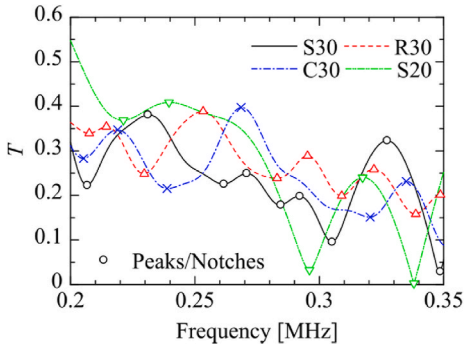

Fig. 11. Frequency dependence of the transmission coefficients for the bonded specimens.

Lamb waves transmitted across the lap joints were measured. The transmission waveforms for specimens S30, R30, C30, and S20 are shown in Fig. 10(a)–(d), respectively. In the waveforms for specimens S30, R30, and C30, i.e. Fig. 10(a)–(c), main wave packets were located at 114 μs. If the guided wave propagating in the overlap region is approximated by the A0 mode in a 4 mm thick homogeneous aluminum alloy plate, the arrival time of the A0 mode at the receiving transducer for the specimens of bond length $L = 30.0$ [mm] is predicted to be 112 μs by using the group velocity. Thus the main wave packets in Fig. 10(a)–(c) appear to correspond to the A0 mode. In a similar manner, the transmitted wave component which traveled via an additional round-trip path along the lap joint is predicted to arrive at 132 μs. This component seems to appear in Fig. 10(a)–(c) but is not clearly distinguishable from the main wave packet. In Fig. 10(d), i.e. the transmission waveform for specimen S20, the first wave packet appeared at 113 μs. By using the group velocity of the A0 mode, the arrival times of the direct wave and the round-trip wave component are predicted as 109 μs and 122 μs, respectively. These two wave components seem to be overlapped in the waveform of Fig. 10(d).

The signals of the transmitted waves including the direct wave and the round-trip waves were extracted together by multiplying tapered rectangular windows, which are shown by dashed lines in Fig. 10(a)–(d). The ranges of the time gates are based on the arrival times of different wave components. The obtained waveforms were analyzed by FFT, and the transmission coefficient was calculated by Eq. (3) for each specimen.

The transmission coefficients for the four bonded specimens are shown together in Fig. 11. The transmission coefficient for each specimen is found to take local maxima and minima at multiple frequencies, which are shown as symbols in the figure. Numerical analyzes in previous studies showed that the local maxima and minima of the transmission coefficient appear due to the constructive and destructive interference of multiply reflected waves generated in the overlap region [11,14]. This trend was qualitatively confirmed in Fig. 11.

Table 4
Estimation results of the tangential bond stiffness K_T for the bonded specimens.

	S30	R30	C30	S20
K_T [GPa/mm]	15	8.1	6.0	17

In the frequency range of 0.2–0.35 MHz, the transmission coefficient for specimen S20 showed two peaks and three notches. On the other hand, the numbers of peaks and notches in specimens S30, R30, and C30 were larger than specimen S20. This feature is likely to be attributed to the shorter bond length of specimen S20. Namely, bonded specimens with longer joint lengths take more local maxima and minima in a fixed frequency range, which are in qualitative agreement with theoretical results. Furthermore, even if the bond lengths are identical, i.e. $L = 30.0$ [mm], the transmission coefficients of specimens S30, R30, and C30 have different sets of peak and notch frequencies. Specimens S30 and R30 had a local minimum at almost the same frequency, 0.208 MHz, but the frequency of the adjacent peak of specimen S30 (0.230 MHz) was higher than that of specimen R30 (0.215 MHz). The peaks and notches of specimen S30 tended to be located at high frequencies compared to the corresponding peaks and notches of specimen R30. It is also found in Fig. 11 that the number of the peaks and notches of specimen C30 is smaller than the other two specimens with $L = 30.0$ [mm], i.e. S30 and R30.

5. Stiffness evaluation results and discussions

In the previous section, it has been shown that the measured transmission coefficients have local maxima and minima. In this section, based on the proposed method described in Section 3.3, the peak and notch frequencies are extracted from the transmission coefficient, and the tangential bond stiffness K_T is evaluated for each bonded specimen. By the minimization of the evaluation function $J(K_T)$, the bond stiffnesses were obtained as in Table 4. The bond stiffnesses K_T estimated for specimens S30 and S20 were almost equal, i.e. $K_T = 15$ [GPa/mm] and

Table 5
Tangential interfacial stiffness K_{IT} for the specimens of bond length $L = 30.0$ [mm].

	S30	R30	C30
K_{IT} [GPa/μm]	0.21	0.033	0.018

$K_T = 17$ [GPa/mm], respectively. This agreement is reasonable because the measured bond thicknesses for specimens S30 and S20 were $h = 0.10$ [mm] and the adherends had been subjected to the same surface pretreatment. As shown by Eq. (6), the bond stiffness K_T is related to the layer stiffness K_{LT} and the interfacial stiffness K_{IT}, which depend on the bond thickness and the adherend surface condition, respectively. The tangential bond stiffness for specimen R30, $K_T = 8.1$ [GPa/mm], was higher than specimen C30, $K_T = 6.0$ [GPa/mm], but was lower than specimen S30 ($K_T = 15$ [GPa/mm]). It is inferred that the sanding of the adherend surfaces increased the bond stiffness K_T.

In order to discuss the effect of the pretreatment, the tangential interfacial stiffness K_{IT} was calculated by substituting the estimated bond stiffness K_T into Eq. (6). The calculated results of the interfacial stiffness K_{IT} for the bonded specimens of $L = 30.0$ [mm] are shown in Table 5. The variation among the interfacial stiffness K_{IT} of the three specimens is found to be more conspicuous than that of the bond stiffness K_T. Among the three specimens, specimen S30 had the highest interfacial stiffness. It was reported in previous studies [6,13], that the sandblasting of adherend surfaces led to the improvement of the interfacial property between adherend and adhesive, which is qualitatively consistent with the present case. The interfacial stiffness of specimen C30 ($K_{IT} = 0.019$ [GPa/μm]) was slightly lower than that of specimen R30 ($K_{IT} = 0.033$ [GPa/μm]). The adherend surface of specimen C30 was contaminated by silicone oil, which probably contributed to the decrease in the interfacial stiffness. To further examine the effect of adherend contamination on the interfacial stiffness, more specimens produced on different conditions should be tested in future work. The detection of the adherend contamination by ultrasonic testing remains an issue, which would depend significantly on the contaminant types and levels [21,22].

In previous studies, the tangential interfacial stiffness of adhesive joints was often examined by measuring reflection spectra for oblique incidence of bulk waves. For example, Baltazar and co-workers [4] estimated the tangential interfacial stiffness of environmentally degraded aluminum alloy adhesive joints as approximately 0.01–3 GPa/μm. The estimated values shown in Table 5 are located within the range of the results reported in the previous study.

By using the estimated values of the tangential bond stiffness K_T in Table 4, the transmission coefficient of the A0 mode was theoretically obtained in the frequency domain for each specimen. The details of the calculation method are described in Ref. [14]. The theoretical transmission coefficients of the A0 mode corresponding to the four bonded specimens are shown in Fig. 12(a)–(d). The peaks and notches of the transmission coefficients are indicated by symbols in the figures. Regarding the peak and notch frequencies, the experimental results are fairly reproduced by the theoretical prediction, which suggests that the peaks and notches of the measured transmission coefficients appeared due to the interference of the transmitted wave components. However, the deviation between the magnitude of the experimental and theoretical transmission coefficients is seen. It is noted that only peak and notch frequencies were utilized in the evaluation procedure of the tangential bond stiffness. In Fig. 12(a)–(d), each curve of the transmission coefficient obtained by the experiment tended to be located below the corresponding theoretical curve in the almost entire frequency range.

Several reasons for the deviation of the magnitude of the transmission coefficients are considered in the theoretical modeling. First, as described in Section 3, the plane strain condition is assumed, and the numerical model is two-dimensional. In the actual measurement, as a wave propagate, the amplitude becomes low due to diffusion attenuation. This geometric effect is not considered in the 2D theoretical analysis and would decrease the magnitude of the measured transmission coefficients. In fact, the measured transmission coefficients tend to be lower than the theoretical results in Fig. 12.

Another reason for the deviation is that the viscoelasticity of the adhesive is not considered in the evaluation procedure. The theoretical

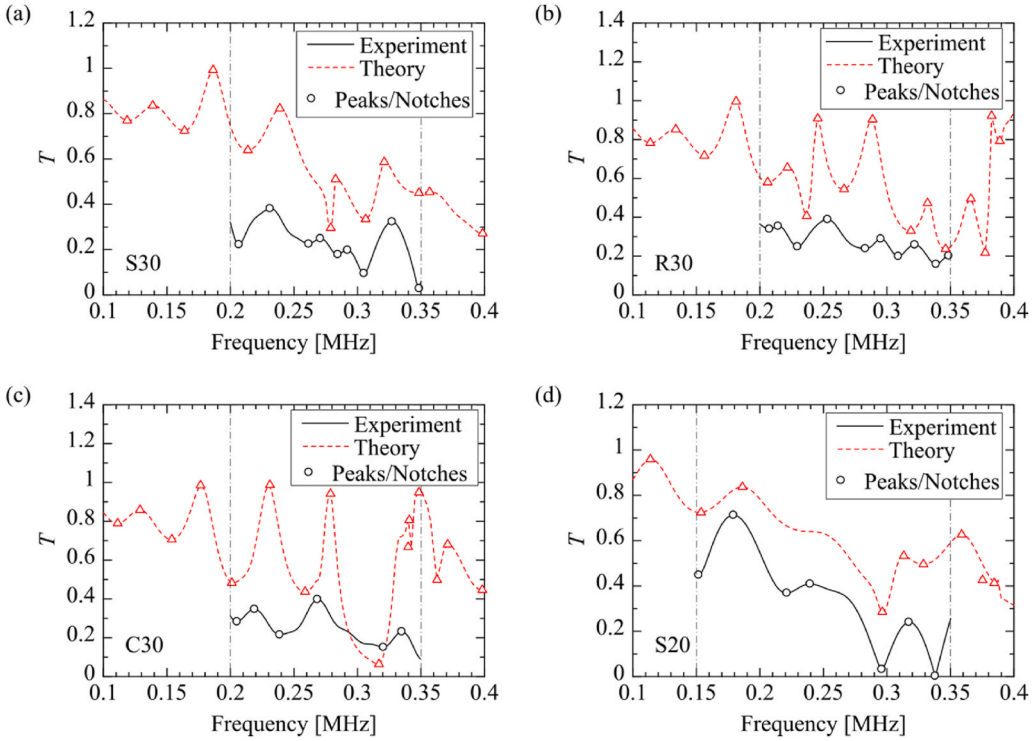

Fig. 12. Measured and estimated transmission coefficients for specimens (a) S30, (b) R30, (c) C30, and (d) S20.

results in Ref. [14] showed that the curves of the transmission coefficients shift lower when considering the viscoelastic attenuation of the adhesive. Accordingly, the peaks and notches of the transmission coefficient get flattened. It is mentioned here again that the viscoelastic damping does not significantly affect the peak and notch frequencies of the transmission coefficients [14]. However, for joints with high viscosity adhesives or/and thick adhesive layers, it would be necessary to examine the damping effect carefully to improve the measurement accuracy.

Finally, the theoretical transmission coefficient is calculated in the frequency domain, i.e. for the incidence of a sinusoidal wave at a single frequency. To observe as sharp peaks and notches as the theoretical curves, the measurement of signals in longer time durations is required. In the actual measurement, however, it is impossible to acquire signals with infinite time durations. The time lengths of the signals available in the evaluation procedure are limited by different factors, such as unnecessary reflections from the side edges of the specimens. If the specimen dimensions were different, this limitation would not be so strict. However, this topic is not further investigated in the present paper.

In the present measurement, the out-of-plane vibrations of the transmitted waves were obtained by the pin-type transducer. As mentioned in Section 2.2, it was confirmed in a preliminary 2D numerical analysis that the transmitted S0 mode does not significantly affect the A0 mode transmission spectra. However, if aforementioned factors, namely, effects of diffusion attenuation, viscoelasticity, and finite signal length are superimposed, whether the effect of the S0 mode is negligible would depend on bonded specimens. This point could be examined by 3D numerical analysis but remains as future work.

6. Conclusions

In this study, the transmission characteristics of Lamb waves for adhesively bonded single lap joints have been examined experimentally, and a tangential bond stiffness evaluation method has been proposed based on the theoretical results. The lowest-order antisymmetric (A0) mode was used as an incident wave, and the measurement was carried out for four bonded specimens with different bonding conditions and bond lengths. Spectral analysis was performed on the waveforms corresponding to the incident and transmitted waves to obtain the transmission coefficient. The experimental results have shown that the transmission coefficient exhibits peaks and notches at multiple frequencies, which are likely to appear owing to the wave interference phenomenon. The four bonded specimens had different sets of peak and notch frequencies. Based on the theoretical results of the Lamb wave transmission characteristics for single lap joints, the tangential bond stiffness has been estimated for each specimen. As a result, the bonded specimens with nominally the same bond thickness and the same adherend pretreatment had almost equal tangential bond stiffness even if the bond lengths were different. Furthermore, the specimens with the sanding of adherend surfaces before bonding showed relatively high interfacial stiffness, while the contamination by silicone oil on adherend surfaces led to the decrease in the interfacial stiffness. This tendency is consistent with the results reported in previous studies, implying the validity of the proposed method.

Acknowledgments

This study has been supported by Grants-in-Aid for Scientific Research (KAKENHI) Grant No. 20K14614 from Japan Society for the Promotion of Science (JSPS). The authors appreciate the constructive comments from the anonymous reviewers.

References

[1] Guyott CC, Cawley P, Adams RD. The non-destructive testing of adhesively bonded structure: a review. J Adhes 1986;20:129–59.
[2] Adams RD, Drinkwater BW. Nondestructive testing of adhesively-bonded joints. NDT E Int 1997;30:93–8.
[3] Lavrentyev AI, Rokhlin SI. Determination of elastic moduli, density, attenuation, and thickness of a layer using ultrasonic spectroscopy at two angles. J Acoust Soc Am 1997;102:3467–77.
[4] Baltazar A, Wang L, Xie B, Rokhlin SI. Inverse ultrasonic determination of imperfect interfaces and bulk properties of a layer between two solids. J Acoust Soc Am 2003;114:1424–34.
[5] Mezil S, Bruno F, Raetz S, Laurent J, Royer D, Prada C. Investigation of interfacial stiffnesses of a tri-layer using zero-group velocity Lamb modes. J Acoust Soc Am 2015;138:3202–9.
[6] Siryabe E, Rénier M, Meziane A, Galy J, Castaings M. Apparent anisotropy of adhesive bonds with weak adhesion and non-destructive evaluation of interfacial properties. Ultrasonics 2017;79:34–51.
[7] Seifried R, Jacobs LJ, Qu J. Propagation of guided waves in adhesive bonded components. NDT E Int 2002;35:317–28.
[8] Ren B, Lissenden CJ. Ultrasonic guided wave inspection of adhesive bonds between composite laminates. Int J Adhes Adhes 2013;45:59–68.
[9] Gauthier C, Galy J, Ech-Cherif El-Kettani M, Leduc D, Izbicki JL. Evaluation of epoxy crosslinking using ultrasonic Lamb waves. Int J Adhes Adhes 2018;80:1–6.
[10] Rokhlin SI. Lamb wave interaction with lap-shear adhesive joints: theory and experiment. J Acoust Soc Am 1991;89:2758–65.
[11] Lowe MJS, Challis RE, Chan CW. The transmission of Lamb waves across adhesively bonded lap joints. J Acoust Soc Am 2000;107:1333–45.
[12] Lanza di Scalea F, Rizzo P, Marzani A. Propagation of ultrasonic guided waves in lap-shear adhesive joints: case of incident a_0 Lamb wave. J Acoust Soc Am 2004;115:146–56.
[13] Castaings M. SH ultrasonic guided waves for the evaluation of interfacial adhesion. Ultrasonics 2014;54:1760–75.
[14] Mori N, Kusaka T. Reflection and transmission characteristics of Lamb waves at an adhesive lap joint of plates. J Acoust Soc Am 2019;145:3075–85.
[15] Golub MV, Eremin AA, Shpak AN, Lammering R. Lamb wave scattering, conversion and resonances in an elastic layered waveguide with a surface-bonded rectangular block. Appl Acoust 2019;155:442–52.
[16] Koodalil D, Rajagopal P, Balasubramaniam K. Bond stiffness estimation with shear horizontal guided waves generated using PPM-EMATs. Int J Adhes Adhes 2021;104:102761.
[17] Jones JP, Whittier JS. Waves at a flexibly bonded interface. J Appl Mech 1964;34:905–9.
[18] Pilarski A, Rose JL. A transverse-wave ultrasonic oblique-incidence technique for interfacial weakness detection in adhesive bonds. J Appl Phys 1988;63:300–7.
[19] Mori N, Matsuda N, Kusaka T. Effect of interfacial adhesion on the ultrasonic interaction with adhesive joints: a theoretical study using spring-type interfaces. J Acoust Soc Am 2019;145:3541–50.
[20] Rose JL. Ultrasonic waves in solid media. Cambridge: Cambridge University Press; 1999.
[21] Dixon S, Edwards C, Palmer SB, Reed J. Considerations for the ultrasonic inspection of metal-adhesive bonds using EMATs. J Nondestr Eval 2000;19:95–103.
[22] Matsuda N, Mori N, Furuta Y, Nishikawa M, Hojo M, Kusaka T. Evaluation of interfacial characteristics of adhesive joints by ultrasonic reflection technique. Proc Meet Acoust 2019:065012.